

Experimental Verification of Nonlinear Position-Flux Zero-Bias Control for Heteropolar Active Magnetic Bearing

Arkadiusz Mystkowski* and Andrzej Kierdelewicz

Bialystok University of Technology, Department of Automatic Control and Robotics, Bialystok, Poland
a.mystkowski@pb.edu.pl, a.kierdelewicz@doktoranci.pb.edu.pl

Abstract — This study presents experimental verification of a nonlinear position-flux control for active magnetic bearing (AMB) system operated with zero-bias flux. Recently developed controllers for nonlinear flux-controlled AMB applications are complicated and inherently difficult to implement. Therefore, three designs of low-order controllers are proposed using nonlinear feedback tools including Lyapunov-based techniques and control Lyapunov functions (CLFs). The control objective is to globally stabilize the rotor mass position in the AMB system. Responses of the AMB system states to initial condition and to external load disturbance are presented and the simulation and experimental results for transient responses are compared. The overshoots are compensated for the zero neighbourhood, and the rotor position amplitude does not exceed 2.5% of the air gap.

Index Terms — Active magnetic bearing, control Lyapunov function, nonlinear flux controller, zero-bias control.

I. INTRODUCTION

The bias-current or bias-flux are frequently used to linearize active magnetic bearing (AMB) dynamics, i.e., see author references [1, 2, 3]. However, large bias-current or bias-flux implies power losses, more heat dissipation and high bearing stiffness. In order to improve the energy efficiency of the AMB system, low- or zero-bias flux control can be applied [4, 5, 6, 7, 8]. The low- or zero-bias flux-controlled AMB dynamics become strongly nonlinear. Therefore, nonlinear control methods based on position-current or position-flux state feedbacks can be applied [9, 10, 11, 12]. In particular, in [10] the uncertain nonlinear flux-controlled AMB system operated with zero-bias is stabilized and so-called *small gain theorem* is used to calculate the robust stability.

The Lyapunov-based technique, such as control Lyapunov function (CLF) was introduced by Artstein and Sontag in 1983 [13, 14]. The idea of CLF-based control is to select a Lyapunov function $V(x)$ and then to try to find a feedback control $u(x)$ that renders $dV(x, u)/dt$, defined negatively. Therefore, for suitable

$V(x)$, we can find a stabilizing control law $u(x)$ for the system feedback [15]. The CLF-based control concept was extended to dynamic systems with known disturbance [16, 17, 18], where $V(x)$ is the RCLF (a robust CLF), if, for a bounded disturbance, ω ensures that $\dot{V}(x, u, \omega) < 0$ [19, 20].

Recently the Lyapunov functions are used in the control application to the AMBs and electric machines. The nonlinear Lyapunov-based observer for the induction motor dynamics with saturation of the iron core is presented [21]. The observer is used to estimate the rotor flux amplitude and phase under varying conditions. The simulation and experimental results show good convergence of the observer comparing with the full-order Luenberger observer. Similarly, in [22] the authors designed a Lyapunov-based fuzzy adaptive controller in order to estimate the dynamic system uncertainties. The adaptive sliding-mode controller is designed for the position of rotor axial direction based on Lyapunov function and radial basis function is given in [23]. Simulations and experimental validation show a promising position tracking of the AMB rotor based on the designed control algorithm under different operating conditions, such as rotor position and force disturbance. The Lyapunov-based model predictive (MPC) scheme for permanent-magnet synchronous machine (PMSM) drive systems is presented in [24]. This system is shown to be asymptotically stable using the convex control set (CCS) input constraint with space vector or pulse width modulation and asymptotically set stable using the finite control set (FCS) input constraint.

The purpose of this paper is to provide the experimental verification of the CLF-based control designs. The experimental results proof that proposed controllers improve the zero-bias flux-controlled AMB performance and are comparable with more complicated approaches, i.e., based on Artstein-Sontag's theorem [4] or passivity-based ideas [5]. In comparison with previous solutions [4, 5], the obtained control laws ensure similar or even better transient responses and better external disturbance attenuation.

The paper is organized as follows. Section 2 presents

a nonlinear one-dimensional AMB model. Section 3 formulates conditions for Lyapunov-based AMB control and proposes CLF-controllers. Section 4 provides simulation of the zero-flux AMB system with CLF states feedbacks. The description of the experimental test rig and experimental results are given in Section 5. Section 6 states the concluding remarks.

II. ZERO-BIAS AMB SYSTEM

Consider a simplified 1-DOF (one-degree-of-freedom) AMB model, that consists of two opposite and presumably identical electromagnets with resistance R_1, R_2 [Ω] and currents i_1, i_2 [A], respectively (see Fig. 1). These electromagnets generate fluxes ϕ_1, ϕ_2 [Wb] and further the attractive forces F_1, F_2 [N], acting on the rotor with mass m [kg]. In order to control the position x [m] of the rotor to the stable state $x = 0$, the voltage inputs of the electromagnets, v_1 and v_2 [V], are used. The cross sectional area of the air-gap is denoted by A [m²] and N is the number of turns of the coil of each electromagnet, respectively.

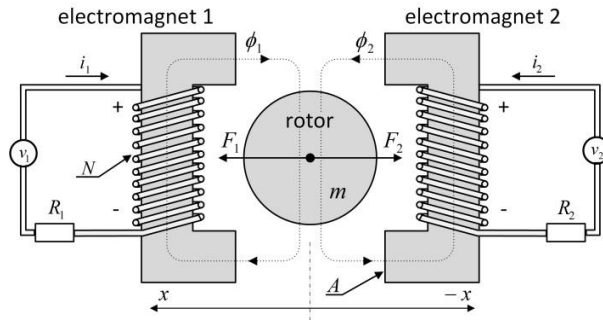


Fig. 1. Simplified one-dimensional AMB.

In order to represent the dynamics of the AMB system operated with zero-bias we follow the approach given in [4, 5]. Let us introduce the following non-dimensionalized state and control variables along with a non-dimensionalized time:

$$\begin{aligned} x_1 &:= \frac{x}{g_0}, x_2 := \frac{\dot{x}}{\Phi_{\text{sat}} \sqrt{g_0 / \mu_0 m A}}, x_3 := \frac{\phi}{\Phi_{\text{sat}}} \\ u &:= \frac{v \sqrt{g_0 \mu_0 m A}}{N \Phi_{\text{sat}}^2}, \tau := t \frac{\Phi_{\text{sat}}}{\sqrt{g_0 \mu_0 m A}}, \end{aligned} \quad (1)$$

where g_0 [m] is the nominal air-gap, \dot{x} [m/s] is the velocity of the rotor mass, $\phi := \phi_1 - \phi_2$ [Wb] is the generalized electromagnetic flux, Φ_{sat} [Wb] is the saturation flux, u is the non-dimensionalized control variable, $v = v_1 - v_2$ [V] is the generalized control voltage, μ_0 is the permeability of free space ($=1.25 \times 10^{-6}$ H/m), τ denotes a non-dimensionalized time, t [s] is the original time.

In zero-bias flux control, the generalized control voltage v changes under the following flux-dependent condition:

$$\begin{aligned} v_1 &= v, \quad v_2 = 0 \quad \text{when } \phi \geq 0, \\ v_2 &= -v, \quad v_1 = 0 \quad \text{when } \phi < 0. \end{aligned} \quad (2)$$

The switching scheme allows us to minimize the control power since at least one of the control voltages v_1 or v_2 and as well as fluxes ϕ_1 or ϕ_2 is zero at the time. The dynamics of the 1-DOF AMB model with zero-bias flux may be presented in terms of (1) as:

$$\begin{cases} \frac{d}{d\tau} x_1 = x_2, \\ \frac{d}{d\tau} x_2 = x_3 |x_3|, \\ \frac{d}{d\tau} x_3 = u. \end{cases} \quad (3)$$

Equation (3) shows that the AMB system has strongly nonlinear dynamics provided by the singularity.

III. LYAPUNOV-BASED AMB CONTROL

In this section we will find the CLF that will make the AMB system globally stable. Consider the continuous-time system:

$$\dot{x} = f(x) + g(x)u, \quad (4)$$

where $u \in \mathbb{R}$ – control input, and vector $f: \mathbb{R}^3 \rightarrow \mathbb{R}^3$ and $g: \mathbb{R}^3 \rightarrow \mathbb{R}^3$, are given by $f(x) = [x_2 \quad x_3^{[2]} \quad 0]^T$, $g(x) = [0 \quad 0 \quad 1]^T$, with $x_3^{[2]} := x_3^2 \text{sgn}(x_3) = x_3 |x_3|$. Recall that system (4) is asymptotically stabilizable with respect to the equilibrium pair (x_0, u_0) , where $x_0 = x(0)$, if there exists a feedback law $u = \alpha(x)$, $\alpha(x_0) = u_0$, defined on a neighbourhood U_{x_0} of x_0 such that α is continuously differentiable on $U_{x_0} \setminus \{x_0\}$, for which the closed-loop system $\dot{x}(t) = (f + \alpha g)(x(t))$ is locally asymptotically stable (with respect to x_0). Recall also that (see [14, 25]) a real continuous function defined on open set $X \subset \mathbb{R}^n$ is a local control Lyapunov function for closed-loop system if it satisfies the following properties:

- (i) V is proper at x_0 , i.e., $\{x \in X: V(x) \leq \varepsilon\}$ is a compact subset of some neighborhood U_{x_0} of x_0 for each sufficiently small $\varepsilon > 0$.
- (ii) V is positive defined on U_{x_0} : $V(x_0) = 0$ and $V(x) > 0$ for each $x \in U_{x_0}$, $x \neq x_0$.
- (iii) $L_f V(x) < 0$ for each $x \neq x_0$, $x \in U_{x_0}$, such that $L_g V(x) = 0$, where $L_g V(x) := \nabla V(x) \cdot g(x)$ denotes the Lie derivative of V with respect to g , and $L_f V(x)$ is the Lie derivative of V with respect to f .

The pair (f, g) of vector fields f and g that satisfies conditions (i)-(iii) is called a *control Lyapunov pair*. If the origin of (4) has CLF, then there exists a control law that renders the system asymptotically stable. We assume that for all $x \neq 0$ there is a positive, proper function $V \in \mathbb{R}_+$ such that:

$$\nabla V(x)[f(x) + g(x)u] < 0. \quad (5)$$

Let us assume that CLF describes the kinetic energy of system (3) is $V = \frac{1}{2}(3x_1^2 + 2x_2^2 + x_3^2)$. Then the

control laws, which fulfil inequality (5), are as follows:

$$\begin{aligned} u_1 &= -3x_1^2x_3 - 2x_2|x_3| - 3x_1x_2x_3 - x_3 + u_0, \\ u_2 &= \frac{1}{2}(3x_1^2 + 2x_2x_3|x_3| + 3x_1x_2 - x_3) + u_0, \quad (6) \\ u_3 &= -x_2|x_3| - x_3 - x_1x_2x_3 + u_0, \end{aligned}$$

where $u_0 = -k_1x_1 - k_2x_2$ with $k_1=0.92$ $k_2=9.94$ were optimized and evaluated earlier in [12]. These gains are kept constant for all simulations and experiments. Regarding Eq. (6), it should be noted that theoretically there are an infinite number of functions. Each of them must to fulfill inequality (5). In our work, we have examined three functions u_1 , u_2 and u_3 that were optimized due the kinetic energy of the system. Detailed information for evaluation of the controller u_1 can be found in [7], u_2 in [6], and u_3 in [8], respectively.

IV. SIMULATION RESULTS

This section presents simulation results obtained for zero-bias AMB system (3), described in Section 2, after applying zero-bias flux control with switching scheme (2). The results are presented for three state-feedback controllers u_1 , u_2 , u_3 (6) and for AMB true states: x [m] position, \dot{x} [m/s] velocity and ϕ [Wb] flux. The AMB specifications are collected in Table 1. All simulations were carried out with sample time of 0.0001 s.

Table 1: AMB specifications

Symbol	Value	Meaning
$ x _{max}$ [m]	0.0002	Rotor position limit
g_0 [m]	0.0004	Nominal width of air-gap
m [kg]	2.5	Rotor mass in the bearing plane
N	60	Number of coil turns
R [Ω]	0.26	Coil resistance
A [m ²]	0.00036	Electromagnet pole area
Φ_{sat} [Wb]	0.0022	Saturation flux
i_{sat} [A]	± 10	Saturation current

The AMB model detailed in Section 2, with parameters given in Table 1 was applied in Matlab/Simulink[®] software, and the control structure is presented in Fig. 2.

The AMB system trajectories and controller outputs are illustrated for the given sinusoidal disturbances d_1 and d_2 with amplitude of ± 1 V and frequency of 10 and 20 Hz respectively, which are constant for all simulations. The disturbance is the external load/force acting on the rotor supported by AMB. This force is used to test the rotor stability. For simplicity we represent the disturbance as voltage. The power amplifier converts this voltage into the disturbance current with amplitude ± 1 A, resulting in the disturbance force generated by the electromagnets. The disturbances d_1 and d_2 are given in Fig. 3.

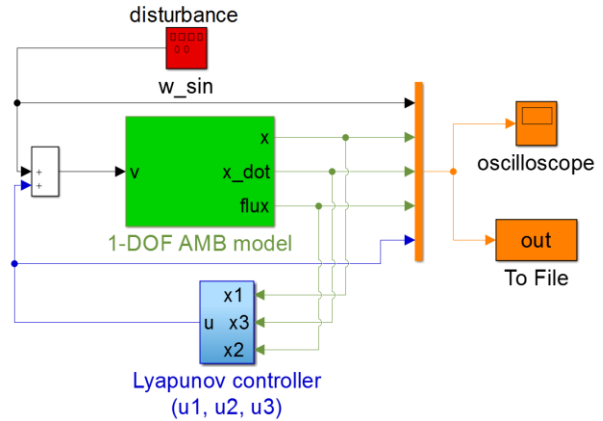


Fig. 2. Simulink control structure.

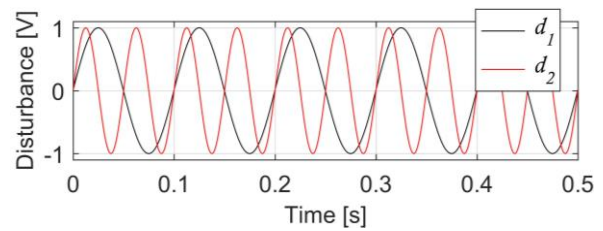


Fig. 3. Sinusoidal disturbances d_1 and d_2 of control voltage.

The AMB state responses to disturbance d_1 , in zero-bias mode with controllers (6) are presented in Fig. 4, respectively. The disturbance d_1 is successfully attenuated by the controller in all cases. The lowest amplitude of the rotor position response is given for controller u_1 , but the flux amplitude is also the highest.

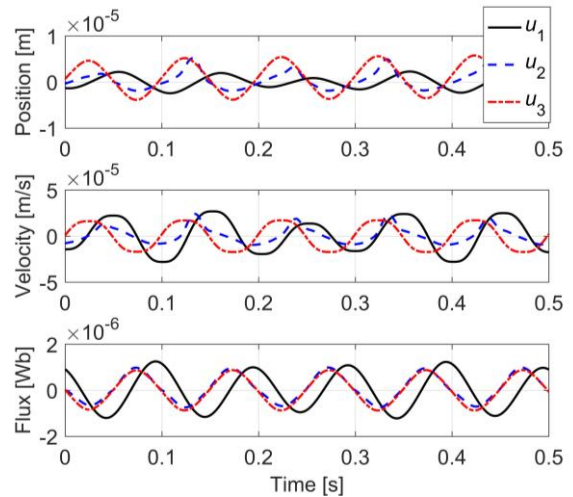


Fig. 4. Responses of closed-loop system with zero-bias to disturbance d_1 employing control laws: u_1 , u_2 and u_3 .

Figure 5 presents the control voltages responses to disturbance d_1 for controllers (6). One can be observed, that the voltage amplitude does not exceed ± 2 V (peak-to-peak). Maximum absolute voltage is about 1.9 V for control law u_2 and minimum equals 0.8 V for u_3 . Although the controller output u_2 has the biggest amplitude (peak-to-peak), the system's response is worse, compared to the controls u_1 and u_3 (see Fig. 4).

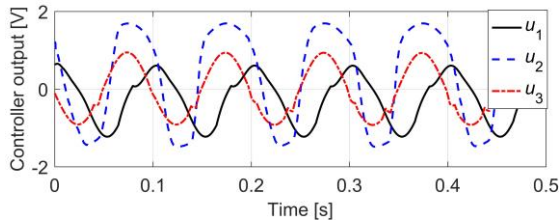


Fig. 5. Comparison of controller outputs responses to disturbance d_1 for controllers u_1, u_2, u_3 .

Comparing control voltages responses given in Fig. 5 with results shown in Fig. 4, we can observe that the shapes of the voltage curves coincide with the rotor displacement values. Similarly with the rotor velocity and flux, which correspond to the displacement values obtained from simulation tests. The smoothest responses were obtained at the lowest values of the control signal. However, the control error was not reduced to zero, while in the case of u_1 and u_2 control, after reaching the extreme position – minimum or maximum, the error was compensated to zero, then again reaching the extreme position and finally stabilize near to zero. According to the assumption, using more electric energy (greater control voltage value) to stabilize the position takes place faster than in the opposite case.

V. EXPERIMENTAL VALIDATION

In this section the performance of the CLF-based AMB state-feedbacks, which simulation results are presented in Section 4, are verified via experimental measurements. The experimental research was carried out using a laboratory stand located in the Bialystok University of Technology where it was designed and fabricated [26].

The AMB system consists of two radial heteropolar active magnetic bearings which support the shaft. The shaft is connected with AC spindle motor by flexible coupling. The total mass of shaft equals 6 kg, and spindle AC motor with inverter enables to the system operated with speed range of 0÷24 000 r/min. The radial AMBs are enclosed by a housing which consists of the stator, two-axes eddy-current displacement sensors, and auxiliary ball bearings. Main components of the experimental test

rig are given in Fig. 6.

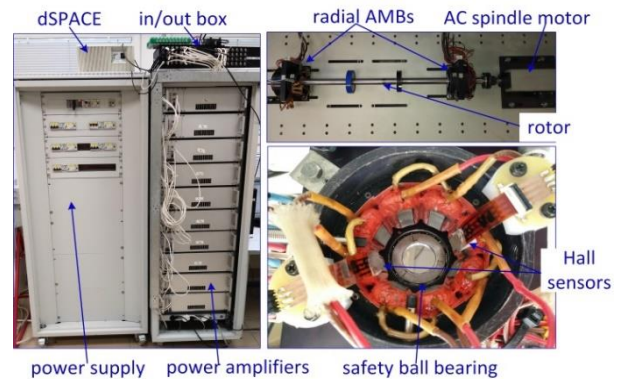


Fig. 6. Experimental setup: PWM power amplifiers, AMB rotor, radial AMB with sensors.

The control laws (6) are implemented in the real-time Digital Signal Processor (DSP) of dSpace. The control algorithms are implemented as the discrete-time models using the Real-Time Interface (RTI) and the Real-Time Workshop (RTW) provided by Matlab/Simulink environment. The signal acquisition is realized using ControlDesk environment of dSPACE. The DSP box consists also 14 bits analog-to-digital (A/D) and digital-to-analog (D/A) converts. The control voltage is the command input signal to the pulse width modulation (PWM) amplifiers. The switching frequency of the PWM amplifiers equals 18 kHz and the PWM voltage is equal to ± 180 V. The PWM amplifiers have inherent current control loops which ensure that the coil current i is proportional to the DSP output voltage command, with the gain 1 A/V. The output control currents which drive the AMB coils are limited to ± 10 A (peak-to-peak) with frequency bandwidth up to 1 kHz. The AMB current noise does not exceed the 0.1 A (peak-to-peak). The radial rotor displacement is measured using contact-less eddy-current sensor with accuracy up to 1 μm . The position sensor output is connected to the proximator converter to ensure stable voltage output which is proportional to the rotor displacement with the gain 7.87 V/mm $\pm 5\%$. The displacement sensor output is filtered using anti-aliasing filters in order to cut-off any noise in the channel above Nyquist frequency (above 2 kHz). In order to obtain rotor velocity, the displacement derivative was used. Noisy signal was smoothed with 1st degree Bessel filter. Flux measurement is provided by ultra-thin (130 μm) Kapton-foil flexible Hall sensors. Two Hall sensors are mounted on opposite poles in the x axis of the AMB. Fabricated conditioning system was used to amplify the Hall voltage outputs. The AMB configuration during measurements and signal connections are shown in Fig. 7.

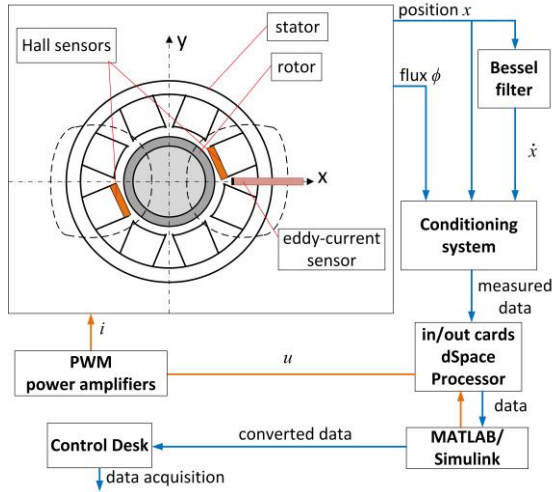


Fig. 7. Measurement configuration.

The experimental tests were divided into two groups: AMB states response to the sinusoidal disturbance d_1/d_2 (presented in Figs. 8÷11) and AMB trajectories response to displacement initial condition $x = 0.0002$ m (given in Figs. 12 and 13). The first set of the results are given for control u_1 . The initial condition response of the AMB system with disturbance d_1 and d_2 is given in Fig. 8. In particular, in Fig. 8 the experimental results are plotted together with simulation responses. According to results given in Fig. 8, it is demonstrated that, the disturbance effect of two different frequencies is compensated with controller voltage output amplitudes.

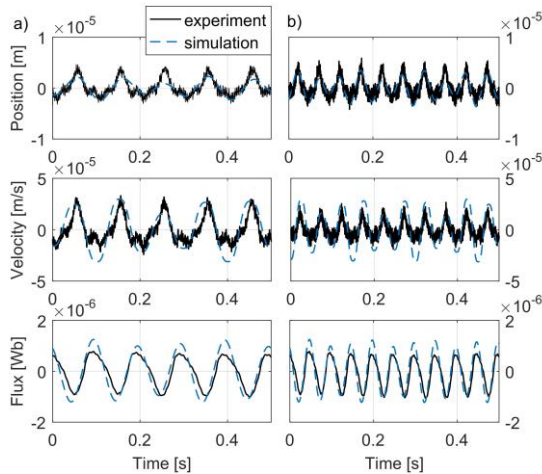


Fig. 8. Comparison of the simulation and experimental transient responses of AMB states with the controller u_1 and disturbances: (a) d_1 ; (b) d_2 .

Figure 9 shows the AMB states responses to disturbance d_1 with control u_2 , and Fig. 10 presents the AMB trajectories for controller u_3 .

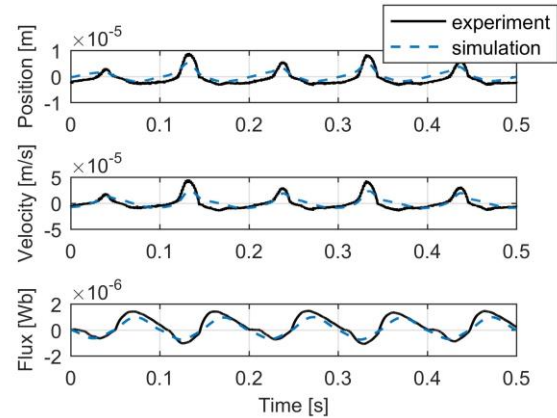


Fig. 9. Experimental and simulation responses of the AMB states to disturbance d_1 with controller u_2 .

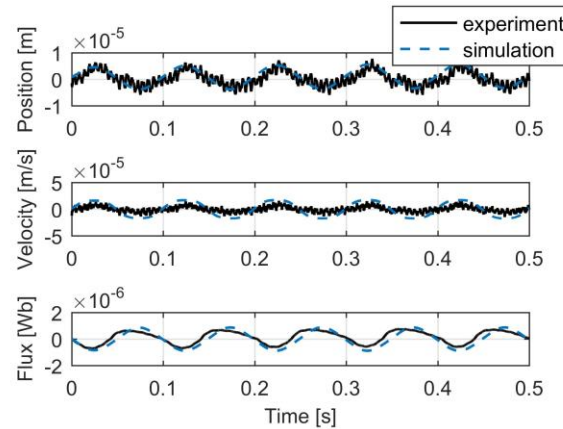


Fig. 10. Experimental and simulation responses of the AMB states to disturbance d_1 with controller u_3 .

The voltage outputs v_1, v_2 for controllers u_1, u_2, u_3 are presented in Fig. 11 in case of both disturbances d_1/d_2 .

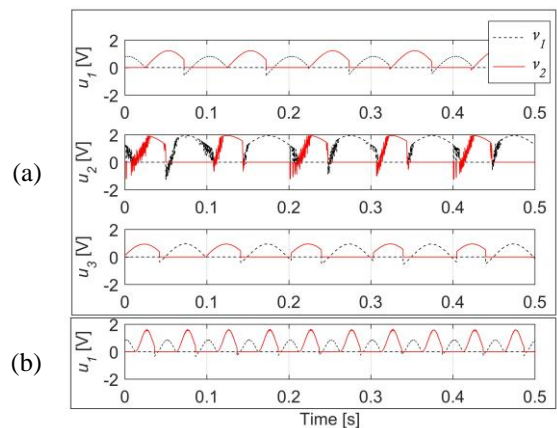


Fig. 11. Control voltages responses to disturbances: (a) d_1 for controllers u_1, u_2, u_3 ; (b) d_2 for controller u_1 .

To summarize, the results presented in Figs. 8–10 indicate that the overshoot is compensated to zero neighbourhood, and the max rotor position amplitude does not exceed $10 \mu\text{m}$ that is 2.5% of the air-gap, despite the desired initial conditions and different disturbances. Moreover, the experimental results of the rotor position responses fit to the simulation one. In the case of u_3 control (Fig. 10), the error is not reduced to zero, but the disturbance is less compensated. In Fig. 11, we can observe the results of the voltage v_1 and v_2 switching operation under the flux-dependent condition (2), where at any given time only one electromagnet is activated. The control voltage amplitude does not exceed 2 V, for controller u_1 , u_2 , and u_3 . The AMB system response to the initial condition, where the rotor is stabilized from the auxiliary bearing (when $x = 0.0002$) to the origin at $x = 0$, is given in Figs. 12 and 13. In particular, Figs. 12 (a) and 12 (b) give the generalized flux ϕ responses and voltage outputs v_1 v_2 responses for controllers u_1 , u_2 and u_3 .

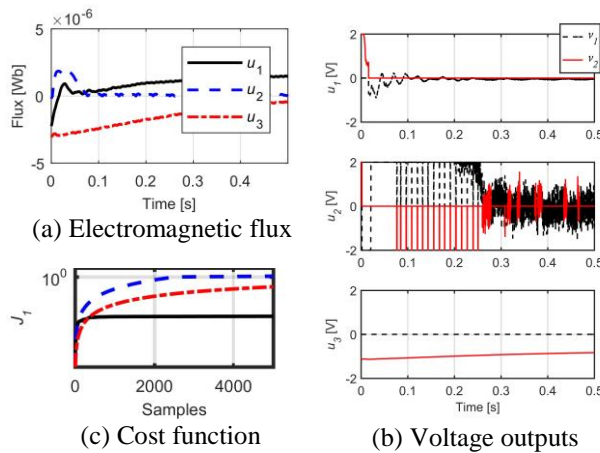


Fig. 12. AMB system responses to the initial condition for controllers u_1 , u_2 , u_3 , without disturbance.

In order to assess the energy requirements for controllers u_1 , u_2 and u_3 , the quadratic cost function of the controller output $J_1 = \int_0^{\infty} u^2 dt$ is used. The cost function for all controllers is compared and results are shown in Figure 12c. One may observe that the highest total energy is required by the controller u_2 . Figure 13 presents comparison of AMB rotor position responses to the initial condition for three controllers: u_1 , u_2 and u_3 .

Stabilization time is less than about 0.1 s for each controller. However the shortest setting time of 0.05 s is achieved with control u_2 , while the setting time of 0.1 s is achieved for controllers u_1 and u_3 with less energy requirements. The energy demand is the lowest in the case of controller u_1 , see Figs. 12 (b) and 12 (c), but the rotor position stabilizes slower (about 0.1 s), see Fig. 13.

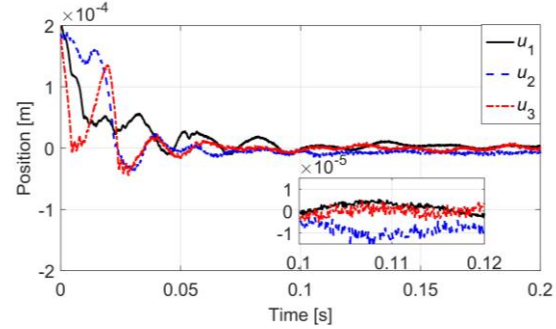


Fig. 13. Comparison of AMB system responses to the initial condition without disturbance.

To conclude the experimental results, we can notice that the zero-bias control design for the AMB is challenging cause of the loss of linear controllability near the origin, when $x = 0$. Thus, in order to produce a low control electromagnetic force we need a large voltage commands v_1 and v_2 , see i.e., output voltages for controller u_2 in Fig. 12. Moreover, we need to notice, that in the experimental measurements, we can observe the influence of the other disturbances which are not addressed (see zoo window in Fig. 13). These disturbances can be divided into external part, i.e., noise in the control voltage and in the measured rotor position or flux, and into internal, such as: self-excited vibrations. The total noise of the measured rotor position is about $1.2 \mu\text{m}$ (peak-to-peak), that is 0.3% of the air-gap. According to the high sensitivity of the AMB rotor dynamics, these disturbances provide to system perturbations and more power consumption.

VI. CONCLUSION

In this paper we have presented three control Lyapunov function (CLF) designs for the flux-controlled AMB system operated with zero-bias. The proposed designs are experimentally validated. The results showed global asymptotic stability of the nonlinear AMB system with the singularity near the origin. The AMB states transient responses to initial condition and to the external load disturbance are presented and compared. The Matlab/Simulink simulation results fit with experimental measurements. Moreover, the low-order CLF-based state controllers gave equivalent results compared with the high-order complex control, i.e., based on Artstein-Sontag's theorem [4]. One of the future goals is to address Lyapunov-based nonlinear feedback controllers for the MIMO system. In the case of 5-DOF AMB flux-controlled rotor dynamics, the decoupling control can be applied.

ACKNOWLEDGMENT

This work is financed by the Polish Ministry of Science and Higher Education (No. S/WM/1/2017).

REFERENCES

- [1] Z. Gosiewski and A. Mystkowski, "Robust control of active magnetic suspension: analytical and experimental results," *Mechanical Systems & Signal Processing*, vol. 22, pp. 1297-1303, 2008.
- [2] A. Mystkowski, "Mu-synthesis for magnetic bearings of flywheel," *Proc. in Applied Mathematics and Mechanics (PAMM)*, Wiley Online Library, vol. 9, pp. 631-632, 2009.
- [3] A. Mystkowski, " μ -synthesis control of flexible modes of AMB rotor," *Acta Mechanica et Automatica*, vol. 4, pp. 83-90, 2010.
- [4] P. Tsiotras and B. C. Wilson, "Zero- and low-bias control designs for active magnetic bearings," *IEEE Trans. Contr. Syst. Technol.*, vol. 11, pp. 889-904, 2003.
- [5] P. Tsiotras and M. Arcak, "Low-bias control of AMB subject to voltage saturation: state-feedback and observer designs," *Proc. of the 41st IEEE Conf. on Decision and Contr.*, Las Vegas, NV, USA, pp. 2474-2479, 10-13 Dec. 2002.
- [6] A. Mystkowski and A. E. Pawluszewicz, "Nonlinear position-flux zero-bias control for AMB system with disturbance," *Applied Computational Electromagnetics Society Journal*, vol. 32, no. 8, pp. 650-656, 2017.
- [7] A. Mystkowski and E. Pawluszewicz, "Remarks on some robust nonlinear observer and state-feedback zero-bias control of AMB," *IEEE The 16th Int. Carpathian Control Conf.*, Szilvásvárad, Hungary, pp. 328-333, 2015.
- [8] A. Mystkowski, E. Pawluszewicz, and R. P. Jastrzebski, "Nonlinear position-flux zero-bias control for AMB system," *IEEE 20th Int. Conf. on Methods and Models in Automation and Robotics*, Międzyzdroje, Poland, pp. 24-27, 24-27 Aug. 2015.
- [9] H. Bleuler, D. Yischer, G. Schweitzer, et al., "New concepts for cost-effective magnetic bearing control," *Automatica*, vol. 30, pp. 871-876, 1994.
- [10] A. Charara, J. De Miras, and B. Caron, "Nonlinear control of a magnetic levitation system without premagnetization," *IEEE Trans. Contr. Syst. Technol.*, vol. 4, pp. 513-523, 1996.
- [11] R. P. Jastrzebski, A. Smirnov, A. Mystkowski, and O. Pyrhönen, "Cascaded position-flux controller for AMB system operating at zero bias," *Energies*, vol. 7, pp. 3561-3575, 2014.
- [12] A. Mystkowski, E. Pawluszewicz, and E. Dragašius, "Robust nonlinear position-flux zero-bias control for uncertain AMB system," *Int. J. of Contr.*, vol. 88, pp. 1619-1629, 2015.
- [13] Z. Artstein, "Stabilization with relaxed controls," *Nonlinear Analysis*, vol. 7, pp. 1163-1173, 1983.
- [14] E. D. Sontag, "A Lyapunov-like characterization of asymptotic controllability," *SIAM Journal of Control and Optimization*, vol. 21, pp. 462-471, 1983.
- [15] E. D. Sontag, "A universal construction of Artstein's theorem on nonlinear stabilization," *Systems and Control Letters*, vol. 13, pp. 117-123, 1989.
- [16] R. A. Freeman and P. V. Kokotović, "Inverse optimality in robust stabilization," *SIAM Journal of Control and Optimization*, vol. 34, pp. 1365-1391, 1996.
- [17] R. A. Freeman and P. V. Kokotović, *Robust Nonlinear Control Design – State–Space and Lyapunov Techniques*, Boston: Birkhäuser, 1996.
- [18] R. A. Freeman and P. V. Kokotović, "Design of 'softer' robust nonlinear control laws," *Automatica*, vol. 29, pp. 1425-1437, 1996.
- [19] F. Clarke, "Lyapunov functions and feedback in nonlinear control, optimal control, stabilization and nonsmooth analysis," *Lecture Notes in Control and Information Science*, vol. 301, pp. 267-282, 2004.
- [20] I. Kanellakopoulos, P. V. Kokotović, and A. S. Morse, "A toolkit for nonlinear feedback design," *Systems and Control Letters*, vol. 18, pp. 83-92, 1992.
- [21] F. Alonge, M. Cirrincione, M. Pucci, and A. Sferlazza, "A nonlinear observer for rotor flux estimation of induction motor considering the estimated magnetization characteristic," *IEEE Trans. on Industry Applications*, vol. 53, no. 6, pp. 5952-5965, 2017.
- [22] J. Fei and J. Zhou, "Robust adaptive control of MEMS triaxial gyroscope using fuzzy compensator," *IEEE Sys., Man, and Cybernetics Society*, vol. 42, no. 6, pp. 1599-1607, 2012.
- [23] H. S. Zad, T. I. Khan, and I. Lazoglu, "Design and adaptive sliding-mode control of hybrid magnetic bearings," *IEEE Trans. on Industrial Electronics*, vol. 65, no. 3, pp. 2537-2547, 2018.
- [24] M. Preindl, "Robust control invariant sets and Lyapunov-based MPC for IPM synchronous motor drives," *IEEE Trans. on Ind. Electronics*, vol. 63, no. 6, pp. 3925-3933, 2016.
- [25] A. Bressan and B. Piccoli, "Introduction to the mathematical theory of control," *Springfield: American Institute of Mathematical Sciences, Applied Math*, vol. 2, 2007.
- [26] Z. Gosiewski and A. Mystkowski, "The robust control of magnetic bearings for rotating machinery," *Solid State Phenomena*, vol. 113, pp. 125-130, 2006.